Polymer Journal (2018) 50:615–625
https://doi.org/10.1038/s41428-018-0072-4

FOCUS REVIEW

Low-bandgap semiconducting polymers based on sulfur-containing phenacene-type molecules for transistor and solar cell applications

Hiroki Mori[1] · Yasushi Nishihara[1]

Received: 18 January 2018 / Revised: 11 April 2018 / Accepted: 12 April 2018 / Published online: 23 May 2018

Abstract

The incorporation of a highly extended π-electron system into a polymer backbone is an effective strategy to develop high-performance donor–acceptor (D–A) polymers suitable for organic electronics because this strategy can facilitate a dense π-π stacking structure, leading to efficient carrier transport. With this in mind, we developed phenanthro[1,2-*b*:8,7-*b*′] dithiophene (PDT) because this new phenacene-type molecule has a highly crystalline nature, deep HOMO level, and high hole mobility, which are characteristics known to be suitable for a donor unit in high-performance D–A polymers. In this focus review, we report recent progress in PDT-containing D-A polymers combined with various strong acceptor units. Incorporation of PDT into a polymer backbone results in deep HOMO energy levels of −5.4~−5.5 eV, strong aggregation, and a dense packing structure with a short π-stacking distance of 3.5~3.6 Å. PDT-based polymers with appropriate alkyl side chains exhibit high hole mobilities of up to 0.18 $cm^2 V^{-1} s^{-1}$ in organic field-effect transistor (OFET) devices due to their tendency to form highly ordered edge-on structures. Furthermore, we can adjust their level of molecular orientation from edge-on to face-on by increasing their molecular weight, leading to a high power conversion efficiency of over 6% in polymer solar cell (PSC) applications. These results demonstrate that PDT is a good candidate as a high-performance building block in D-A polymers.

Introduction

Organic field-effect transistors (OFETs) and polymer solar cells (PSCs) are next-generation electronic devices because they can replace conventional silicon technologies owing to their potential features, such as low-cost and low-energy production, light weight, flexible characteristics, and use in wearable devices [1–4]. Among developed organic semiconductors, donor–acceptor (D–A) polymers consisting of electron-donating and electron-deficient aromatic rings (Fig. 1a) have been widely recognized as significant molecules for developing high-performance OFETs and PSCs [5–11]. The push-pull effect of D–A polymers facilitates electron delocalization and the construction of quinoidal structures through a mesomeric effect. Thus, broad absorption with a reduced energy gap (E_g) and strong intermolecular interactions due to the Coulombic interactions between conjugated backbones can be obtained (Fig. 1b) [5, 6, 8, 10]. These features can provide a strong light-harvesting ability, high charge carrier mobility, and highly ordered thin-film structures [5–11]. In terms of the design of high-performance D–A polymers, the following general strategy is suggested. The electronic structures of D–A polymers are strongly determined by the highest occupied molecular orbital (HOMO) energy level of the donor unit and the lowest unoccupied molecular orbital (LUMO) of the acceptor unit (Fig. 1c) [5, 6, 8], and we can easily control the HOMO and LUMO energy levels of D–A polymers by modifying the various donor and acceptor units. Furthermore, structural features, including the backbone shape, position and shape of the side chains, and symmetry of each building block, strongly affect the crystallinity, molecular orientation, and π-stacking distance and, thus, the polymer carrier transport capacity [12–19]. Therefore, a careful combination of appropriate donor and acceptor units is essential to optimize the performance of D–A polymers in organic electronics.

✉ Yasushi Nishihara
ynishiha@okayama-u.ac.jp

[1] Research Institute for Interdisciplinary Science, Okayama University, 3-1-1 Tsushimanaka, Kita-ku, Okayama 700-8530, Japan

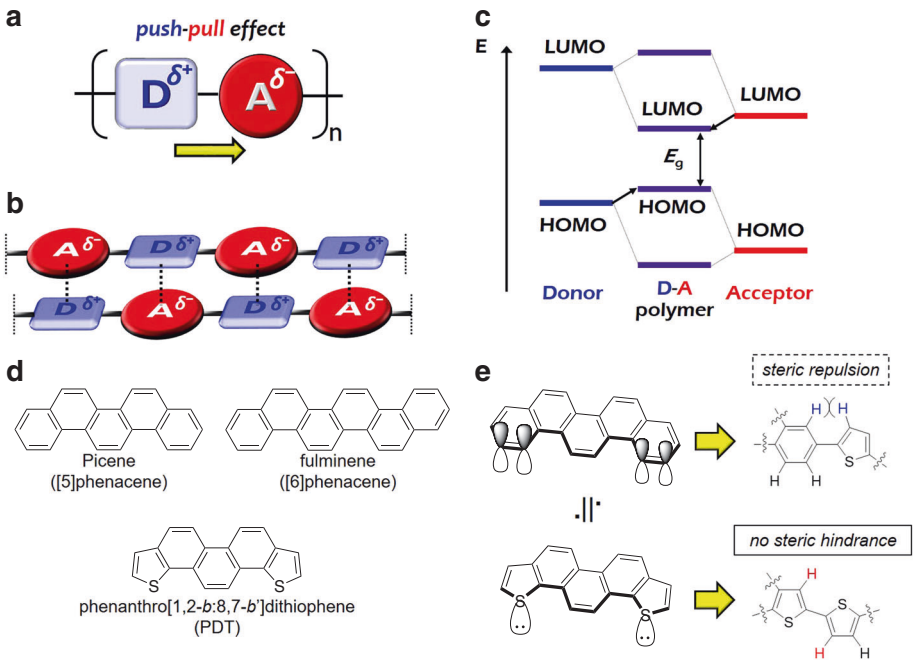

Fig. 1 Schematic images of the (**a**) D–A polymers, (**b**) electrostatic interactions, and (**c**) HOMO and LUMO energy levels of the D-A polymers. **d** Chemical structures of the [*n*] phenacenes and PDT. **e** Schematic diagrams of the isoelectronic structures and steric repulsion of picene and PDT

To produce high-performance OFETs and PSCs, the most important issue is the construction of dense π-π stacking with a long-range ordered structure in the solid state, which enables efficient carrier transport along the intermolecular π-stacking direction and/or intramolecular polymer main chain, leading to a high carrier mobility in OFETs and a high fill factor (FF) in PSCs [13, 14, 20–22]. Among a number of design strategies, one method to achieve such a highly oriented structure in the solid state is to incorporate extended π-electron cores in a polymer backbone, which can provide strong intermolecular interactions and a high crystallinity. In addition, the existence of a large π-plane can promote particularly effective π-orbital overlap, leading to a strongly self-assembly nature with short π-stacking distances (3.5~3.7 Å) and minimal conformational disorder [9, 13, 14]. Polymers containing π-extended aromatic cores also have a high thermal stability owing to their rigid and planar backbone. Indeed, D–A polymers based on cores with over four fused aromatic rings, such as naphthodithiophene [23, 24], tetrathienoacene [25], dithienobenzodithiophene [26], naphthobisthiadiazole [11, 18], and thienobenzothiophene isoindigo [27], show high field-effect hole mobilities in OFETs or good photovoltaic performances in PSCs. However, such π-extended molecule-based polymers are still limited by their multi-step synthesis and difficult selective functionalization in the late stage. In addition, controlling the molecular orientation, crystallinity, and thin-film morphology is difficult because the incorporation of a π-extended core into the polymer backbone drastically reduces the solubility of the polymer. Therefore, the development of new building units with efficient synthesis methods is highly important for developing high-performance polymeric semiconductors in organic electronics.

[*n*]Phenacenes, such as picene ([5]phenacene) and fulminene ([6]phenacene), are well known as representative p-type semiconductors in OFETs (Fig. 1d) [28–31]. In general, π-extension by increasing the number of fused rings generally elevates the HOMO energy level of organic molecules. However, [*n*]phenacenes have deep HOMO energy levels of approximately −5.8 eV [32, 33], which result in high chemical and air stabilities. This phenomenon has been explained in detail by several researchers from a theoretical viewpoint [34, 35]. Moreover, π-extended [*n*] phenacenes can facilitate densely packed herringbone structures in thin films, leading to a high hole mobility of over 1 $cm^2 V^{-1} s^{-1}$ [28–31]. However, when [*n*]phenacenes are incorporated into a polymer backbone, there are two significant problems. First, selective functionalization at the terminal benzene ring of picene is very difficult, requiring a multi-step synthesis [32, 33, 36]. Second, the large steric repulsion between the terminal benzene rings of the [*n*] phenacenes and the neighboring π-cores produces a highly twisted backbone (Fig. 1e), which prevents effective π-orbital overlap and results in poor packing structures and a poor OFET performance [9, 37]. Focusing on a superior hole-transport ability and excellent chemical stability in air, we designed a new picene analogue, phenanthro[1,2-*b*:8,7-*b*′]dithiophene (PDT, Fig. 1d), by replacing the terminal benzene rings with thiophene rings. Very recently, we developed PDT as a new p-type semiconductor for OFETs with an efficient gram-scale synthetic route [38, 39]. This

new picene-type molecule has several advantages. For example, 2,9-functionalized PDT can easily be synthesized because of the high acidity at the α-positions of the terminal thiophene rings and has a deep HOMO energy level of −5.6 eV, which is similar to that of picene, and results in a high air stability [38]. In addition to its rigid, planar π-framework, highly delocalized HOMO orbital, and its high coplanarity due to the absence of steric hindrance between the terminal thiophene rings of PDT and the neighboring aromatic cores, the structure (Fig. 1e) can enhance the effective π-orbital overlap between neighboring molecules to construct a highly crystalline and densely packed structure that shows a high hole mobility of up to 0.11 $cm^2 V^{-1} s^{-1}$ [38]. Therefore, PDT is a potential donor unit for high-performance D–A polymers in organic electronics.

This focus review describes recent progress in the design of PDT-based D–A polymers and the application of these polymers to organic electronics involving OFETs and PSCs. The relationship between their device performance and thin-film structures is also discussed.

PDT-diketopyrrolopyrrole copolymers: First synthesis of PDT-based D–A polymers

Among several combinations of donor and acceptor units, the weak donor-strong acceptor concept results in ideal HOMO and LUMO energy levels for D–A polymers [6, 40] because the concept can yield the desired low-lying HOMO energy level, broad absorption in the visible region, and a high air stability. A weak donor unit, PDT, was first combined with diketopyrrolopyrrole (DPP) as an acceptor unit, which is a well-known strong acceptor for high-performance D–A polymers [41].

PDT was synthesized by sequential Negishi coupling, epoxidation, and $InCl_3$-catalyzed cycloaromatization [39]. Then, stannylation of PDT with *n*-BuLi and trimethylstannyl chloride gave the corresponding PDT monomer. **P-PDT-DPP-R** (R denotes the branched alkyl chains, Fig. 2a) was synthesized by Migita-Kosugi-Stille coupling with the corresponding PDT and DPP monomers [42]. The **P-PDT-DPP-R** polymers have a high thermal stability, strong aggregation behavior, and dense packing structure with a short π-stacking distance of 3.5~3.6 Å, indicating that the incorporation of a rigid and π-extended PDT framework into the polymer main chain can enhance the intermolecular interactions. Interestingly, the compounds exhibited significantly extended absorption spectra up to 1000 nm with a very narrow bandgap of ca. 1.2 eV in the solid state. However, conventional solar cells with the device configuration of ITO/(PEDOT:PSS)/**P-PDT-DPP-R**:$PC_{61}BM$/Ca (10 nm)/Al (80 nm) yielded a low power conversion efficiency (PCE) value of up to 2.03% for **P-PDT-DPP-DT** (**DT** denotes 2-decyltetradecyl) and 0.83% for **P-PDT-DPP-DP** (**DP** denotes 3-decylpentadecyl). Moreover, the fabricated **P-PDT-DPP-DT** and **P-PDT-DPP-DP**-based OFETs exhibited moderate hole mobilities of 1.0×10^{-2} and 9.2×10^{-3} $cm^2 V^{-1} s^{-1}$, respectively. One of the possible reasons for the poor performance of the **P-DPP-DPP-R** polymers is their low solubility due to their strong intermolecular interactions, which limit their molecular weight. The actual number-average molecular weights (M_n) of the two PDT-DPP polymers could not be determined because of their strong aggregation tendencies even in a high-temperature solution. However, both polymers are soluble in hot chloroform, and broad peaks were also observed in the longer retention time regions in gel-permeation chromatography. From these results, we speculated that the molecular weights of the two polymers are rather low, i.e., oligomers. Such oligomeric features and their strong aggregation tendency prevented crystallization into an ordered structure in OFETs and promoted large-scale phase separation of the

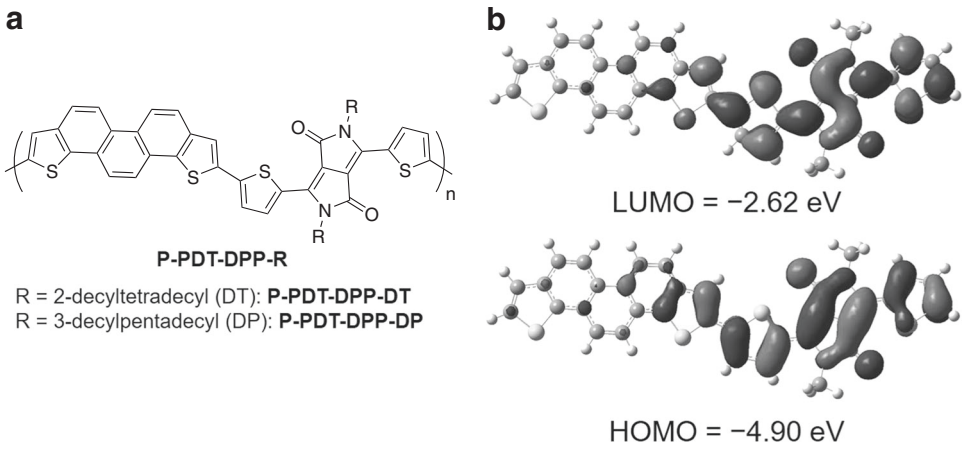

Fig. 2 **a** Chemical structures of **P-PDT-DPP-R** and the (**b**) HOMO and LUMO geometries of **P-PDT-DPP-R** calculated from DFT (B3LYP/6-31 G(d))

blended films with $PC_{61}BM$ in PSCs, leading to less effective carrier transport and charge separation [43, 44]. In addition, since the HOMO coefficients of **P-PDT-DPP-R** are localized on the DPP framework (Fig. 2b), the effective π-conjugation significantly elevated the HOMO energy levels to approximately −5.2 eV [45], which led to a low V_{oc} of down to 0.65 V [46]. Thus, further optimization, including the side chains and choice of appropriate strong acceptor units, is essential for achieving high-performance electronics.

PDT-isoindigo copolymers: effect of the length and topology of the side chains on the solar cell performance and molecular ordering

P-PDT-DPP-R polymers have some superior features as described above, but some critical improvements are required, as follows: (i) appropriate acceptor units to maintain the low-lying HOMO energy levels (HOMO delocalization over the entire molecule); (ii) increased number of alkyl side chains to ensure an adequate solubility and molecular weight. To address these issues, bis(alkylthienyl)isoindigo (IID) was selected as an appropriate acceptor for PDT-based D-A polymers [47]. IID is a well-known functional dye and strong electron-acceptor in D-A molecules with low-lying HOMO and LUMO energy levels owing to the strong electron affinity of its two lactam moieties in the IID core [48]. When such an IID core is combined with PDT as a weak electron-donating unit, the HOMO is efficiently delocalized over the entire molecule, leading to a deeper HOMO energy level than that of the **P-PDT-DPP-R** polymers (Fig. 3c). In addition, four alkyl side chains can be installed on the *N*-position of the IID core and the β-position of the neighboring thiophenes, which can improve the solubility and molecular weight. In most cases, the length, topology, and number of side chains strongly affect the morphology and molecular orientation [12–14]. Therefore, optimization of the side chains can control the phase separation structure and molecular orientation, which can also provide additional knowledge concerning the structure-property relationship. With these issues in mind, five PDT-IID copolymers (**P-PDT-IID-R^{1}R^2**, R^1 denotes linear or branched alkyl chains on thiophene rings and R^2 denotes branched alkyl chains on the *N*-position of an IID unit; abbreviated nomenclature of the polymers is shown in Fig. 3a) with different alkyl side chains were designed and synthesized [47]. Alkyl side chains with similar carbon numbers were chosen to facilitate a face-on orientation, as suggested in published reports [49].

Since the PDT-IID copolymer **1DT** has poor solubility, it cannot form a uniform thin film, resulting in no photovoltaic response due to short circuiting. However, the other four copolymers with long alkyl side chains have enough solubility to allow their inclusion as working components of solar cell devices. All polymers showed a broad absorption up to 780 nm with energy gaps of 1.6~1.7 eV. From the temperature-dependent UV-vis absorption spectra in solution, **12OD** and **BOBO**, with shorter alkyl chains, have stronger intermolecular interactions than **12DT** and **HDHD**, with longer alkyl chains. In particular, **BOBO** formed large aggregates, even in a high-temperature solution. The polymers with all branched alkyl chains (HOMO = −5.50 eV for **BOBO** and −5.51 eV for **HDHD**) tended to have deeper HOMO energy levels than the polymers with linear and branched alkyl chains (−5.45 eV for both **12OD** and **12DT**).

Inverted solar cells with the device structure of ITO/ZnO/(**P-PDT-IID-R^{1}R^2**:$PC_{71}BM$)/MoO_3 (6 nm)/Ag (50 nm) were fabricated and characterized. The solar cells based on **12OD** and **BOBO** with shorter alkyl chains showed better PCEs of up to 5.06% (J_{sc} = 9.99 mA cm^{-2}, V_{oc} = 0.80 V, FF = 0.63) and 5.28% (J_{sc} = 10.70 mA cm^{-2}, V_{oc} = 0.82 V, FF = 0.60), respectively, while the **12DT** and **HDHD**-based cells with longer alkyl chains exhibited poor PCEs of up to 3.10% (J_{sc} = 6.63 mA cm^{-2}, V_{oc} = 0.82 V, FF = 0.57) and 1.09% (J_{sc} = 2.05 mA cm^{-2}, V_{oc} = 0.90 V, FF = 0.59), respectively. From the grazing incidence wide-angle X-ray scattering (GIWAXS) analyses of blended films with PCBM, all polymers showed first or second-order (*h*00) diffraction on the q_z axis and weak (010) diffraction (Figs. 3d–g). These results indicate that all the polymers formed structures with predominant edge-on orientation (Fig. 3b), which is not favorable for efficient carrier transport in PSCs [13, 14]. Interestingly, the face-on ratios of **12DT** and **HDHD** were 0.08 and 0.41, respectively, which are higher than those of the corresponding polymers **12OD** (0.03) and **BOBO** (0.12) with shorter alkyl chains. Although polymers **12DT** and **HDHD**, with longer alkyl chains, assembled with better molecular orientations, significantly lower performances were observed. This is due to the lower molecular weight and smaller intermolecular interactions of **12DT** and **HDHD**, which promote large phase separations, resulting in poor charge separation and carrier transport and, thus, a poor PCE [44]. In the case of polymers with shorter alkyl chains, **12OD** and **BOBO** formed a well-separated structure with an appropriate interpenetrating network, leading to efficient carrier transport and charge separation. Although **BOBO** has longer π-stacking (3.7 Å) than **12OD** (3.6 Å), **BOBO** formed a better molecular orientation with a slightly higher face-on ratio and almost amorphous structure than that of **12OD**. The slightly better structural orientation of **BOBO** can enhance the carrier transport efficiency, resulting in a slightly higher J_{sc}. However, the PCE difference between **12OD** and

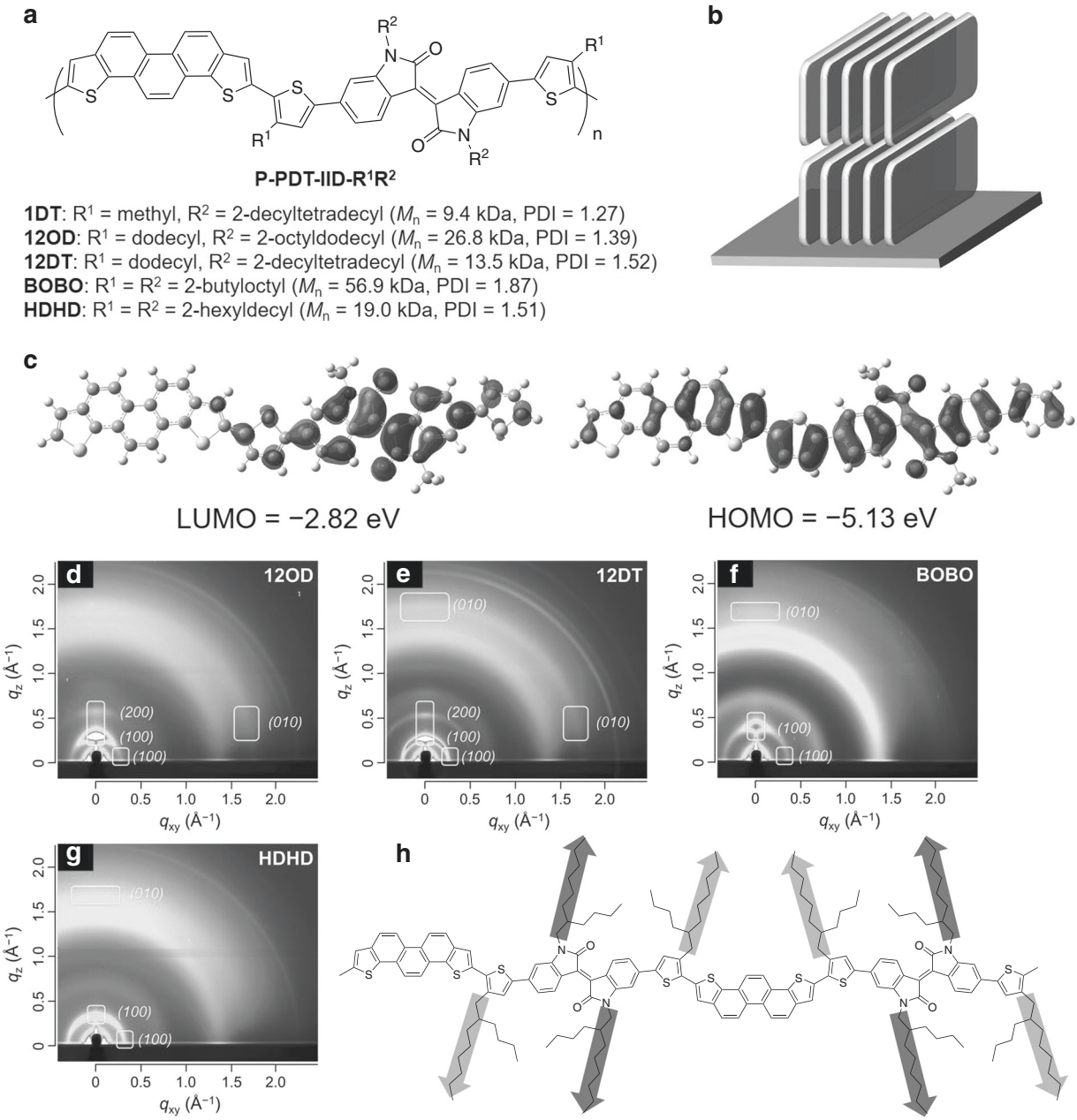

Fig. 3 **a** Chemical structures of **P-PDT-IID-R^{1}R^2** and **b** schematic images of the edge-on orientation. **c** HOMO and LUMO geometries of **P-PDT-IID-R^{1}R^2** calculated from DFT (B3LYP/6-31 G(d)). GIWAXS images of **P-PDT-IID-R^{1}R^2**/$PC_{61}BM$ blended films; **d** **12OD**, **e** **12DT**, **f** **BOBO**, and **g** **HDHD** [47]. **h** Proposed polymer structure of **BOBO** [47]. Reprinted with permission from ref. 47. Copyright (2015) American Chemical Society

BOBO was not as large, which was likely due to their almost amorphous nature, as evident from their weak diffraction in the blended films. One possible reason for the low-crystalline nature of all the PDT-IID systems may be the axisymmetrical structure of PDT, which reduces the regularity of the polymer backbone. Since the alkyl side chains do not point in the same direction in the PDT-IID copolymers, there was less π-π overlap and a less ordered structure (Fig. 3h) [47].

PDT-isoindigo copolymers: effect of the side chains on the transistor performance and molecular ordering

Most PDT-IID copolymers preferentially form with an edge-on orientation, which is a suitable structure for efficient carrier transport parallel to the substrate [13, 14, 22]. This indicates that PDT-IID copolymers may have a high potential for use in OFET devices. To evaluate their

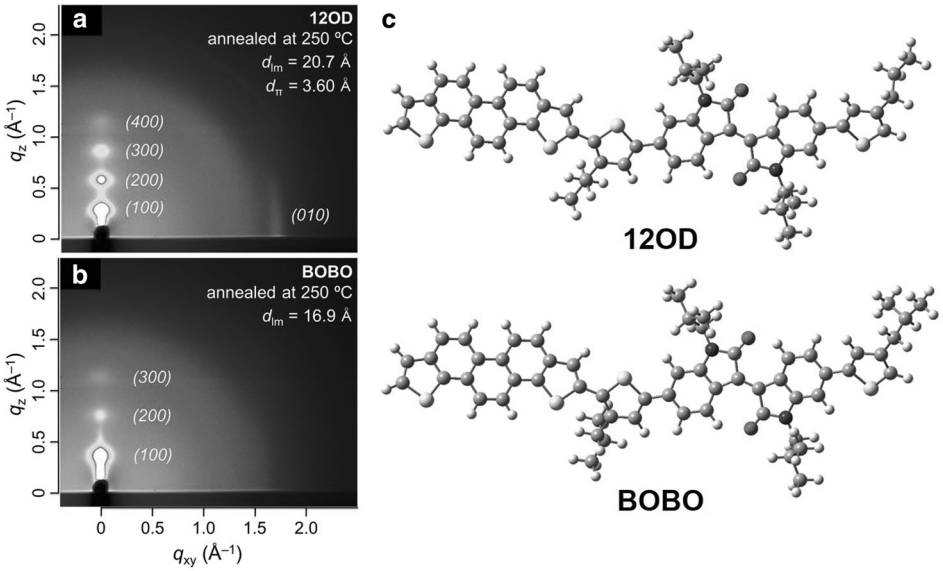

Fig. 4 GIWAXS images of (**a**) **12OD** and (**b**) **BOBO** films on an FOTS-treated n^+-Si/SiO_2 substrate annealed at 250 °C [50]. **c** Calculated structures of a model compound. Structural optimization was performed by B3LYP/6-31 G(d). Linear and branched alkyl chains were replaced with *n*-propyl and isobutyl groups, respectively [50]. Reproduced with permission from Ref. 50. Copyright (2015) Chemical Society of Japan

potential for OFETs and to further explore their structure-property relationships, typical OFET devices were fabricated and characterized [50]. In these devices, **12OD** and **BOBO**, which show a strong intermolecular interaction, were used as the active layer.

Typical bottom gate-top contact OFET devices were fabricated and characterized. Either 1*H*,1*H*,2*H*,2*H*-tridecafluorooctyltriethoxysilane (FOTS) or octadecyltriethoxysilane (ODTS) was used as the self-assembled monolayer. The hole mobilities of both polymer-based OFETs increased with the increasing thermal annealing temperature, and the maximum hole mobility was produced by annealing at 250 °C. In the case of **12OD**, the hole mobility reached 0.11 (for FOTS) and 0.16 $cm^2 V^{-1} s^{-1}$ (for ODTS). In contrast, the **BOBO**-based OFETs showed ca. 2-3 times lower hole mobilities (0.052 for FOTS and 0.041 $cm^2 V^{-1} s^{-1}$ for ODTS) than those of the **12OD**-based devices. This is strongly attributable to their thin-film structure, as indicated by the following evidence. From the GIWAXS images of the **12OD** film on an n^+-Si/SiO_2 substrate (Fig. 4a), fourth-order (*h*00) diffractions were observed as spots on the q_z axis and (010) diffraction as a short arc on the q_{xy} axis, which indicated the existence of a highly ordered edge-on orientation. In contrast, the **BOBO** thin film showed only three orders of (*h*00) diffraction on the q_z axis (Fig. 4b). These diffraction patterns showed that **BOBO** also formed the edge-on orientation, but its crystallinity was significantly lower than that of **12OD**. The weakly crystalline nature of **BOBO** significantly reduced the efficient carrier transport parallel to the substrate, resulting in a lower hole mobility. The optimized geometry of a model compound calculated by DFT (B3LYP/6-31 G(d)) indicated that **12OD** and **BOBO** have almost the same coplanarity (Fig. 4c). However, the partial alkyl moiety of the branched side chains in **BOBO** pointed in a direction orthogonal to the polymer backbone (Fig. 4c). The presence of such sterically hindered side chains prevents effective π-orbital overlap between the polymer backbones, leading to a less ordered structure in the solid state [50].

Dependence of PDT-IID copolymer solar cell performance on molecular weight and molecular ordering

In developing high-performance D-A polymers for solar cells, controlling the molecular weight is also a critical issue. For instance, polymers with a high M_n show a better miscibility with soluble C_{60}, which can provide a well-separated and appropriate interpenetrating network [51]. In other cases, high M_n polymers can crystallize into a microphase separation structure because the aggregation tendency of polymers increases with M_n [51]. Thus, cells based on typical high-M_n polymers show higher PCEs than cells based on low-M_n polymers, owing to the enhanced J_{sc} and FF. Moreover, controlling the molecular weight can change the molecular orientation, but few examples of this have been reported [52–54].

For these reasons, we focused on controlling the M_n in the PDT-IID system. Copolymer **12OD** showed a good solar cell performance with a PCE of over 5%, but it has a low-crystalline nature and predominantly edge-on orientation, which limit its solar cell performance. One possible reason for its low crystallinity may be its relatively low M_n (~26.8 kDa). To improve its PSC performance, high-M_n **12OD** was synthesized and characterized [55].

Typically, in a Migita-Kosugi-Stille coupling polymerization, many factors, such as the purity, stability, and

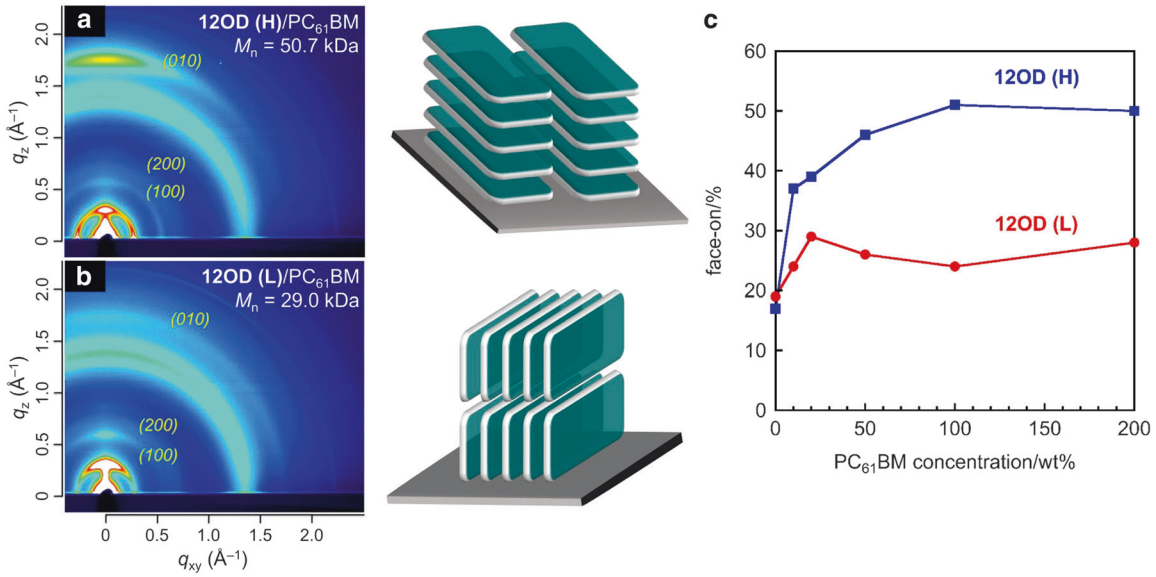

Fig. 5 GIWAXS patterns of the **12OD**-based films blended with $PC_{61}BM$: **a 12OD (H)** and **b 12OD (L)** [55]. **c** Calculated face-on ratio of **12OD** films with different concentrations of $PC_{61}BM$ [55]. Reprinted with permission from ref. 55. Copyright (2017) American Chemical Society

stoichiometry of the monomers, strongly affect the M_n of the polymer [56]. Thus, both PDT and IID monomers were carefully purified by triple recrystallization. When polymerization was performed with highly purified monomers, high-M_n **12OD** (~50.7 kDa) was obtained, which was double the M_n of the previously synthesized **12OD**. By controlling the polymerization temperature and time, we obtained low-molecular-weight **12OD** with a M_n (~29.0 kDa) similar to that of the previously synthesized **12OD** ($M_n = 26.8$ kDa). Herein, **12OD (L)** and **12OD (H)** denote the low-molecular-weight and high-molecular-weight polymers, respectively.

UV-vis absorption and cyclic voltammetry revealed that **12OD (L)** and **12OD (H)** have the same energy gap of ca. 1.6 eV and a HOMO energy level of approximately −5.4 eV. In the low-M_n **12OD** (29.0 kDa) synthesized in this work, the fabricated solar cells showed a lower PCE of 3.51% with the same V_{oc} and FF as that of the previously synthesized **12OD** ($M_n = 26.8$ kDa), although both low-M_n **12OD** had comparable molecular orientations, crystallinities, and phase separation structures. One possible reason for the difference in the OPV performances is batch-to-batch deviation, which may change the optimal conditions, such as the optimal thickness and p/n ratios. In fact, the **12OD** (29.0 kDa) synthesized in this work has a slightly higher solubility than that of the previously synthesized **12OD** ($M_n = 26.8$ kDa), which may affect the thin-film structure. On the other hand, a **12OD (H)**/$PC_{61}BM$-based inverted solar cell exhibited a higher PCE (5.88%) with the same V_{oc} (0.81 V) and FF (0.68) and higher J_{sc} (10.68 mA cm^{-2}) than a **12OD (L)**/$PC_{61}BM$-based cell (PCE = 3.51%, $J_{sc} = 6.51$ mA cm^{-2}, $V_{oc} = 0.80$ V, FF = 0.68). In addition, when $PC_{71}BM$ was used as the *n*-type semiconductor, a **12OD (H)**-based solar cell showed a further increase in the PCE of up to 6.11%.

To understand these differences, a GIWAXS analysis was performed. The GIWAXS analyses revealed that the **12OD (H)**/$PC_{61}BM$ film formed a face-on orientation with a long-range ordered structure (Fig. 5a), while a low-crystalline edge-on structure was observed in the blended film of **12OD (L)**/$PC_{61}BM$ (Fig. 5b). The high crystallinity and ideal molecular orientation could promote light harvesting and hole transport ability, resulting in a high J_{sc} and excellent PCE. To further explore the reasons for the change in the molecular orientation of **12OD (H)**, GIWAXS analyses with different blend ratios were performed. Before the addition of $PC_{61}BM$, both **12OD (L)** and **12OD (H)** predominantly formed an edge-on orientation with almost the same crystallinity. After the addition of $PC_{61}BM$, the molecular ordering of **12OD (L)** gradually decreased, but no significant change in the face-on ratio was observed with any blend ratio (Fig. 5c). In contrast, the face-on crystallite of **12OD (H)** was gradually enriched by increasing the blend ratio of $PC_{61}BM$. When an equimolar amount of $PC_{61}BM$ was added, **12OD (H)** formed a highly ordered face-on orientation with long-range order. The detailed GIWAXS analysis indicated that the orientation change of **12OD (H)** was induced by the addition of $PC_{61}BM$. We speculate that the strong aggregation ability of **12OD (H)** can drive the crystallization and active interaction with $PC_{61}BM$ to form a face-on orientation [13].

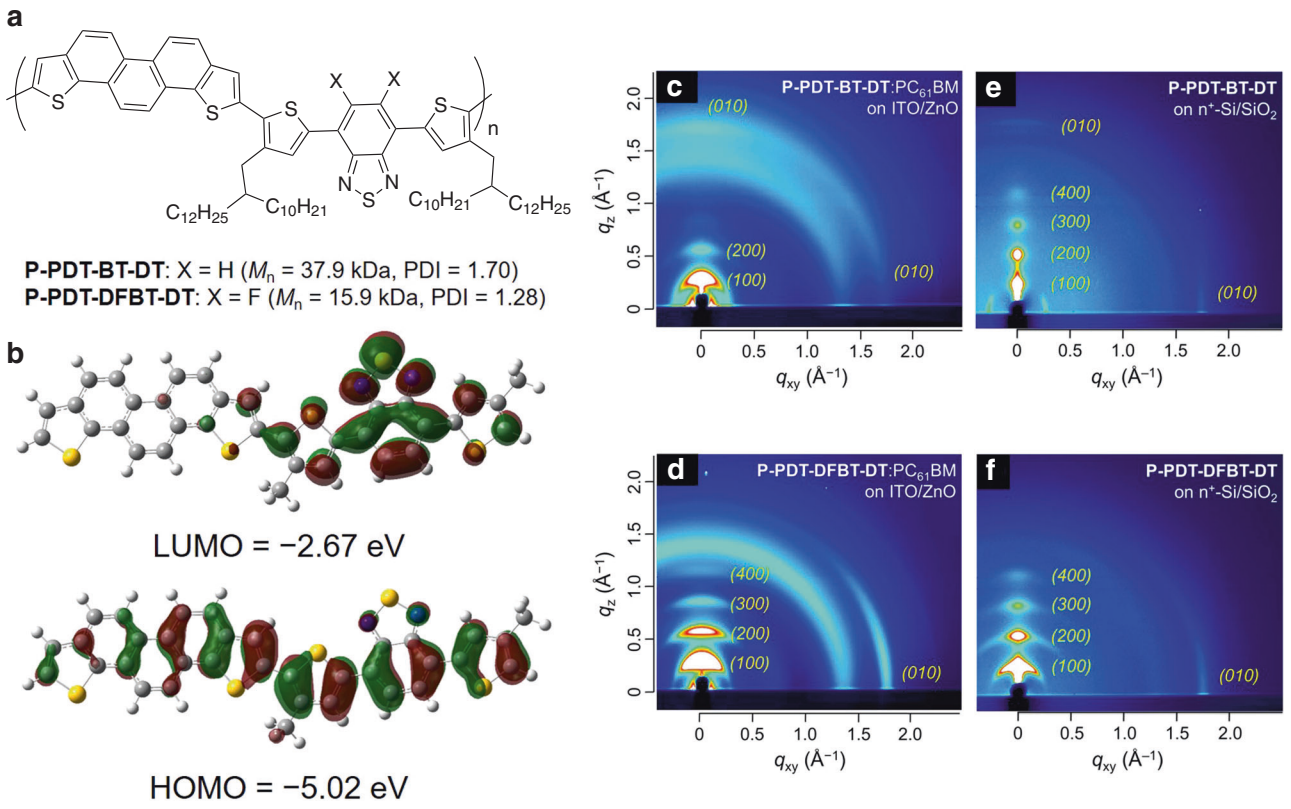

Fig. 6 **a** Chemical structures of **P-PDT-(DF)BT-DT**. **b** HOMO and LUMO geometries of **P-PDT-BT-DT** calculated from DFT (B3LYP/6-31 G(d)). GIWAXS patterns of polymer films blended with $PC_{61}BM$ on an ITO/ZnO substrate; **c** **P-PDT-BT-DT** and **d** **P-PDT-DFBT-DT** [59]. GIWAXS patterns of polymer films on an n^+-Si/SiO_2 substrate; **e** **P-PDT-BT-DT** and **f** **P-PDT-DFBT-DT** [59]. Reproduced from ref. 59. with permission from The Royal Society of Chemistry

PDT-benzothiadiazole (BT) copolymers: development of high-crystallinity D–A polymers

Because typical dyes/pigments such as DPP and IID have a strongly polarized core, they dramatically enhance intermolecular interactions [41, 48]. In this case, bulky or additional side chains are required to ensure enough solubility, but they often lead to less effective π-π overlap and a low crystallinity. In order to overcome this problem, benzothiadiazole (BT) was chosen as the acceptor unit. BT is a well-known electron-acceptor unit in high-performance organic electronics with a strong electron affinity and deep HOMO energy level owing to the electron-poor nature of the thiadiazole ring and the *o*-benzoquinoidal structure of the BT unit [6, 8, 45, 57]. In combination with PDT, the HOMO coefficients delocalize over the end of the PDT moiety, which is similar to the case of IID, leading to a deep HOMO energy level, as is evident from the DFT calculation (Fig. 6b). Incorporation of a non-polar BT core into a PDT-based polymer backbone can provide a sufficient solubility without bulky or additional solubilizing groups. Furthermore, the C_{2v} symmetry of the BT core can increase the regularity of the polymer backbone, which can enhance the effective π-π overlap to yield high-crystallinity films [14, 18, 58]. In view of these effects, two PDT-BT copolymers (**P-PDT-(DF)BT-DT**, DFBT denotes 5,6-difluorobenzothiadiazole, Fig. 6a) were designed and synthesized [59].

P-PDT-BT-DT and **P-PDT-DFBT-DT** have strong intermolecular interactions and sufficiently deep HOMO energy levels of −5.28 and −5.42 eV and relatively small energy gaps of 1.63 and 1.65 eV, respectively. Although the fluorine-substituted polymer **P-PDT-DFBT-DT** showed stronger aggregation behavior than the non-fluorinated polymer **P-PDT-BT-DT** due to its higher coplanarity [60], it also had a limited solubility, leading to a low molecular weight (~15.9 kDa). Inverted PSCs based on **P-PDT-BT-DT** and **P-PDT-DFBT-DT** showed low PCEs of up to 3.48% (J_{sc} = 7.35 mA cm^{-2}, V_{oc} = 0.71 V, FF = 0.67) and 3.79% (J_{sc} = 7.96 mA cm^{-2}, V_{oc} = 0.81 V, FF = 0.59), respectively, but they formed appropriate microphase separation structures. The GIWAXS analysis revealed that both polymers formed well-ordered thin film structures with a predominantly edge-on arrangement (Figs. 6c, d). In particular, more pronounced and high-order (*h*00)

diffraction signals were observed in the blended film of **P-PDT-DFBT-DT**. In addition, the π-stacking distance of **P-PDT-DFBT-DT** (3.53 Å) was shorter than that of **P-PDT-BT-DT** (3.63 Å). Furthermore, **P-PDT-DFBT-DT** formed a denser packing structure with long-range order due to its stronger intermolecular interactions. However, the highly crystalline edge-on orientation limited carrier transport in both PSCs, resulting in low J_{sc} values below 8 mA cm^{-2} and low PCEs [13, 14].

In OFET devices, both **P-PDT-BT-DT** and **P-PDT-DFBT-DT** formed highly crystalline edge-on orientations when polymer films were thermally annealed at 250 or 300 °C (Fig. 6e, f). However, the face-on orientation also coexisted in the **P-PDT-BT-DT** film, leading to a lower hole mobility of up to 0.072 cm^2 V^{-1} s^{-1}. On the other hand, a **P-PDT-DFBT-DT**-based OFET showed a high hole mobility of up to 0.18 cm^2 V^{-1} s^{-1} due to the formation of a highly crystalline and densely packed structure with an optimal arrangement, which can promote efficient carrier transport in OFETs [13, 22]. These results imply that an increase in regularity can enhance the π-orbital overlap between polymer backbones, leading to a high crystallinity. Such a highly crystalline and well-ordered structure is very beneficial for high-performance D–A polymers, showing that PDT has high potential as a construction unit in D–A polymers. Thus, the PDT-DFBT copolymer could be one of the more promising candidates for high-performance electronics.

Conclusion

This focus review has described our recent progress in investigating phenanthrodithiophene (PDT)-based D-A polymers as a new class of p-type semiconductors for OFETs and PSCs. Additionally, the relationship between the detailed thin-film structure and device properties was discussed, leading to a new strategy for molecular design. By optimizing the combination of a strong acceptor unit with side chains, PDT-based polymers can provide optimal energy levels with sufficiently deep HOMO energy levels of −5.4~−5.5 eV, strong aggregation tendencies, and densely packed structures with short π-stacking distances of 3.5-3.6 Å, originating from the rigid and highly π-extended PDT framework. Their strong self-assembling nature yields a highly ordered edge-on orientation in the solid state, leading to high hole mobilities of up to 0.18 cm^2 V^{-1} s^{-1} in OFET devices. In addition, an increase in the molecular weight can change the molecular orientation from edge-on to a fully face-on structure, which was induced by the addition of $PC_{61}BM$, resulting in high PCEs of over 6%. These results demonstrate that PDT has high potential as an electron donor in high-performance D–A polymers.

Acknowledgements This study was supported by ACT-C, JST Grant Number JPMJCR12YW, Japan; JSPS Grant-in-Aid for Young Scientists B (No. 26810129); Grant-in-Aid for Scientific Research on Innovative Areas, MEXT, Grant Number 15 H00751, Japan; Okayama Foundation for Science and Technology; Shorai Foundation for Science; and the Electric Technology Research Foundation of Chugoku. The GIWAXS experiments were performed at BL46XU of SPring-8 with the approval of the Japan Synchrotron Radiation Research Institute (JASRI) (Proposals 2014A1530, 2014B1583, 2014B1915, 2016A1542, and 2016B1875). We thank Prof. Itaru Osaka (Hiroshima University) and Dr. Tomoyuki Koganezawa (JASRI) for the GIWAXS image measurements and Ms. M. Kosaka and Mr. M. Kobayashi at the Department of Instrumental Analysis, Advanced Science Research Center, Okayama University for the elemental analyses measurements. The SC-NMR Laboratory at Okayama University is gratefully acknowledged for the NMR spectral measurements.

Compliance with ethical standards

Conflict of interest The authors declare that they have no conflict of interest.

References

1. Yan H, Chen Z, Zheng Y, Newman C, Quinn JR, Dötz F, Kastler M, Facchetti A. A high-mobility electron-transporting polymer for printed transistors. Nature. 2009;457:679–87.
2. Han S-T, Peng H, Sun Q, Venkatesh S, Chung K-S, Lau SC, Zhou Y, Roy VAL. An overview of the development of flexible sensors. Adv Mater. 2017;29:1700375.
3. Lipomi DJ, Bao Z. Stretchable, elastic materials and devices for solar energy conversion. Energy Environ Sci. 2011;4:3314–28.
4. Espinosa N, Laurent A, Krebs FC. Ecodesign of organic photovoltaic modules from Danish and Chinese perspectives. Energy Environ Sci. 2015;8:2537–50.
5. Cheng Y-J, Yang S-H, Hsu C-S. Synthesis of conjugated polymers for organic solar cell applications. Chem Rev. 2009;109:5868–923.
6. Zhou H, Yang L, You W. Rational design of high performance conjugated polymers for organic solar cells. Macromolecules. 2012;45:607–32.
7. He Y, Hong W, Li Y. New building blocks for π-conjugated polymer semiconductors for organic thin film transistors and photovoltaics. J Mater Chem C. 2014;2:8651–61.
8. Lu L, Zheng T, Wu Q, Schneider AM, Zhao D, Yu L. Recent advances in bulk heterojunction polymer solar cells. Chem Rev. 2015;115:12666–731.
9. Holliday S, Donaghey JE, McCulloch I. Advances in charge carrier mobilities of semiconducting polymers used in organic transistors. Chem Mater. 2014;26:647–63.
10. Guo X, Facchetti A, Marks TJ. Imide- and amide-functionalized polymer semiconductors. Chem Rev. 2015;114:8943–9021.
11. Osaka I. Semiconducting polymers based on electron-deficient π-building units. Polym J. 2015;47:18–25.
12. Mei J, Bao Z. Side chain engineering in solution-processable conjugated polymers. Chem Mater. 2014;26:604–15.
13. Osaka I, Takimiya K. Backbone orientation in semiconducting polymers. Polymer. 2015;59:A1–15.
14. Marszalek T, Li M, Pisula W. Design directed self-assembly of donor–acceptor polymers. Chem Commun. 2016;52:10938–47.
15. Kim J-H, Park JB, Jung IH, Grimsdale AC, Yoon SC, Yang H, Hwang D-H. Well-controlled thieno[3,4-*c*]pyrrole-4,6-(5*H*)-dione based conjugated polymers for high performance organic

photovoltaic cells with the power conversion efficiency exceeding 9%. Energy Environ Sci. 2015;8:2352–6.
16. Zhou N, Guo X, Ortiz RP, Harschneck T, Manley EF, Lou SJ, Hartnett PE, Yu X, Horwitz NE, Burrezo PM, Aldrich TJ, Navarrete JTL, Wasielewski MR, Chen LX, Chang RPH, Facchetti A, Marks TJ. Marked consequences of systematic oligothiophene catenation in thieno[3,4-*c*]pyrrole-4,6-dione and bithiopheneimide photovoltaic copolymers. J Am Chem Soc. 2015;137:12565–79.
17. Lee W, Kim G-H, Ko S-J, Yum S, Hwang S, Cho S, Shin Y-H, Kim JY, Woo HY. Semicrystalline D−A copolymers with different chain curvature for applications in polymer optoelectronic devices. Macromolecules. 2014;47:1604–12.
18. Osaka I, Shimawaki M, Mori H, Doi I, Miyazaki E, Koganezawa T, Takimiya K. Synthesis, characterization, and transistor and solar cell applications of a naphthobisthiadiazole-based semiconducting polymer. J Am Chem Soc. 2012;134:3498–507.
19. Hu H, Jiang K, Yang G, Liu J, Li Z, Lin H, Liu Y, Zhao J, Zhang J, Huang F, Qu Y, Ma W, Yan H. Terthiophene-based D−A polymer with an asymmetric arrangement of alkyl chains that enables efficient polymer solar cells. J Am Chem Soc. 2015;137:14149–57.
20. Guo X, Zhou N, Lou SJ, Smith J, Tice DB, Hennek JW, Ortiz RP, Navarrete JTL, Li S, Strzalka J, Chen LX, Chang RPH, Facchetti A, Marks TJ. Polymer solar cells with enhanced fill factors. Nat Photonics. 2013;7:825–33.
21. Jao M-H, Liao H-C, Su W-F. Achieving a high fill factor for organic solar cells. J Mater Chem A. 2016;4:5784–801.
22. Sirringhaus H, Brown PJ, Friend RH, Nielsen MM, Bechgaard K, Langeveld-Voss BMW, Spiering AJH, Janssen RAJ, Meijer EW, Herwig P, de Leeuw DM. Two-dimensional charge transport in self-organized, high-mobility conjugated polymers. Nature. 1999;401:685–8.
23. Osaka I, Kakara T, Takemura N, Koganezawa T, Takimiya K. Naphthodithiophene−naphthobisthiadiazole copolymers for solar cells: alkylation drives the polymer backbone flat and promotes efficiency. J Am Chem Soc. 2013;135:8834–7.
24. Osaka I, Abe T, Shimawaki M, Koganezawa T, Takimiya K. Naphthodithiophene-based donor−acceptor polymers: versatile semiconductors for OFETs and OPVs. ACS Macro Lett. 2012;1:437–40.
25. Matthews JR, Niu W, Tandia A, Wallace AL, Hu J, Lee W-Y, Giri G, Mannsfeld SCB, Xie Y, Cai S, Fong HH, Bao Z, He M. Scalable synthesis of fused thiophene-diketopyrrolopyrrole semiconducting polymers processed from nonchlorinated solvents into high performance thin film transistors. Chem Mater. 2013;25:782–9.
26. Park S, Lim BT, Kim B, Son HJ, Chung DS. High mobility polymer based on a π-extended benzodithiophene and its application for fast switching transistor and high gain photoconductor. Sci Rep. 2014;4:5482.
27. Yue W, Ashraf RS, Nielsen CB, Collado-Fregoso E, Niazi MR, Yousaf SA, Kirkus M, Chen H-Y, Amassian A, Durrant JR, McCulloch I. A thieno[3,2-*b*][1]benzothiophene isoindigo building block for additive- and annealing-free high-performance polymer solar cells. Adv Mater. 2015;27:4702–7.
28. Okamoto H, Kawasaki N, Kaji Y, Kubozono Y, Fujiwara A, Yamaji M. Air-assisted high-performance field-effect transistor with thin films of picene. J Am Chem Soc. 2008;130:10470–1.
29. Okamoto H, Hamao S, Goto H, Sakai Y, Izumi M, Gohda S, Kubozono Y, Eguchi R. Transistor application of alkyl-substituted picene. Sci Rep. 2014;4:5048.
30. Komura N, Goto H, He X, Kitamura H, Eguchi R, Kaji Y, Okamoto H, Sugawara Y, Gohda S, Sato K, Kubozono Y. Characteristics of [6]phenacene thin film field-effect transistor. Appl Phys Lett. 2012;101:083301.
31. Kubozono Y, He X, Hamao S, Teranishi K, Goto H, Eguchi R, Kambe T, Gohda S & Nishihara Y. Transistor application of phenacene molecules and their characteristics. Eur J Inorg Chem. 2014;2014:3806–19.
32. Mori H, Chen X-C, Chang N-H, Hamao S, Kubozono Y, Nakajima K, Nishihara Y. Synthesis of methoxy-substituted picenes: substitution position effect on their electronic and single-crystal structures. J Org Chem. 2014;79:4973–83.
33. Chang N-H, Mori H, Chen X-C, Okuda Y, Okamoto T, Nishihara Y. Synthesis of substituted [6]phenacenes through Suzuki-Miyaura coupling of polyhalobenzene with alkenylboronates and sequential intramolecular cyclization via C–H bond activation. Chem Lett. 2013;42:1257–9.
34. Suresh CH, Gadre SR. Clar's aromatic sextet theory revisited via molecular electrostatic potential topography. J Org Chem. 1999;64:2505–12.
35. Poater J, Visser R, Solà M, Bickelhaupt FM. Polycyclic benzenoids: why kinked is more stable than straight. J Org Chem. 2007;72:1134–42.
36. Kubozono Y, Mitamura H, Lee X, He X, Yamanari Y, Takahashi Y, Suzuki Y, Kaji Y, Eguchi R, Akaike K, Kambe T, Okamoto H, Fujiwara A, Kato T, Kosugi T, Aoki H. Metal-intercalated aromatic hydrocarbons: a new class of carbon-based superconductors. Phys Chem Chem Phys. 2011;13:16476–93.
37. Osaka I, Abe T, Shinamura S, Miyazaki E, Takimiya K. High-mobility semiconducting naphthodithiophene copolymers. J Am Chem Soc. 2010;132:5000–1.
38. Nishihara Y, Kinoshita M, Hyodo K, Okuda Y, Eguchi R, Goto H, Hamao S, Takabayashi Y, Kubozono Y. Phenanthro[1,2-*b*:8,7-*b′*]dithiophene: a new picene-type molecule for transistor applications. RSC Adv. 2013;3:19341–7.
39. Hyodo K, Nonobe H, Nishinaga S, Nishihara Y. Synthesis of 2,9-dialkylated phenanthro[1,2-*b*:8,7-*b*']dithiophenes via cross-coupling reactions and sequential Lewis acid-catalyzed regioselective cycloaromatization of epoxide. Tetrahedron Lett. 2014;55:4002–5.
40. Zhou H, Yang L, Stoneking S, You Y. A weak donor-strong acceptor strategy to design ideal polymers for organic solar cells. ACS Appl Mater Interfaces. 2010;2:1377–83.
41. Yi Z, Wang S, Liu Y. Design of high-mobility diketopyrrolopyrrole-based π-conjugated copolymers for organic thin-film transistor. Adv Mater. 2015;27:3589–606.
42. Mori H, Suetsugu M, Nishinaga S, Chang N-H, Nonobe H, Okuda Y, Nishihara Y. Synthesis, characterization, and solar cell and transistor applications of phenanthro[1,2-*b*:8,7-*b′*] dithiophene–diketopyrrolopyrrole semiconducting polymers. J Polym Sci Part A Pol Chem. 2015;53:709–18.
43. Tsao HN, Cho DM, Park I, Hansen MR, Mavrinskiy A, Yoon DY, Graf R, Pisula W, Spiess HW, Müllen K. Ultrahigh mobility in polymer field-effect transistors by design. J Am Chem Soc. 2011;133:2605–12.
44. Heeger AJ. 25th Anniversary article: bulk heterojunction solar cells: understanding the mechanism of operation. Adv Mater. 2014;26:10–28.
45. Takimiya K, Osaka I, Nakano M. π-Building blocks for organic electronics: revaluation of "inductive" and "resonance" effects of π-electron deficient units. Chem Mater. 2014;26:587–93.
46. Scharber MC, Mühlbacher D, Koppe M, Denk P, Waldauf, Heeger AJ, Brabec CJ. Design rules for donors in bulk-heterojunction solar cells—towards 10% energy-conversion efficiency. Adv Mater. 2006;18:789–94.
47. Nishinaga S, Mori H, Nishihara Y. Phenanthrodithiophene−isoindigo copolymers: effect of side chains on their molecular order and solar cell performance. Macromolecules. 2015;48:2875–85.
48. Wang E, Mammo W, Andersson MR. 25th Anniversary article: isoindigo-based polymers and small molecules for bulk

heterojunction solar cells and field effect transistors. Adv Mater. 2014;26:1801–26.
49. Osaka I, Saito M, Koganezawa T, Takimiya K. Thiophene–thiazolothiazole copolymers: significant impact of side chain composition on backbone orientation and solar cell performances. Adv Mater. 2014;26:331–8.
50. Nishinaga S, Mori H, Nishihara Y. Impact of alkyl side chains on thin-film transistor performances in phenanthrodithiophene-isoindigo copolymers. Chem Lett. 2015;44:998–1000.
51. Katsouras A, Gasparini N, Koulogiannis C, Spanos M, Ameri T, Brabec CJ, Chochos CL, Avgeropoulos A. Systematic analysis of polymer molecular weight influence on the organic photovoltaic performance. Macromol Rapid Commun. 2015;36:1778–97.
52. Fukuta S, Seo J, Lee H, Kim H, Kim Y, Ree M, Higashihara T. 2,2′-Bis(1,3,4-thiadiazole)-based π-conjugated copolymers for organic photovoltaics with exceeding 8% and its molecular weight dependence of device performance. Macromolecules. 2017; 50:891–9.
53. Osaka I, Saito M, Mori H, Koganezawa T, Takimiya K. Drastic change of molecular orientation in a thiazolothiazole copolymer by molecular-weight control and blending with $PC_{61}BM$ leads to high efficiencies in solar cells. Adv Mater. 2012;24:425–30.
54. Li W, Yang L, Tumbleston JR, Yan L, Ade H, You W. Controlling molecular weight of a high efficiency donor-acceptor conjugated polymer and understanding its significant impact on photovoltaic properties. Adv Mater. 2014;26:4456–62.
55. Mori H, Hara S, Nishinaga S, Nishihara Y. Solar cell performance of phenanthrodithiophene−isoindigo copolymers depends on their thin-film structure and molecular weight. Macromolecules. 2017;50:4639–48.
56. Carsten B, He F, Son HJ, Xu T, Yu L. Stille polycondensation for synthesis of functional materials. Chem Rev. 2011;111: 1493–528.
57. Parker TC, Patel DG, Moudgil K, Barlow S, Risko C, Brédas J-L, Reynolds JR, Marder SR. Heteroannulated acceptors based on benzothiadiazole. Mater Horiz. 2015;2:22–36.
58. Ying L, Hsu BBY, Zhan H, Welch GC, Zalar P, Perez LA, Kramer EJ, Nguyen T-Q, Heeger AJ, Wong W-Y, Bazan GC. Regioregular pyridal[2,1,3]thiadiazole π-conjugated copolymers. J Am Chem Soc. 2011;133:18538–41.
59. Mori H, Nonobe H, Nishihara Y. Highly crystalline, low band-gap semiconducting polymers based on phenanthrodithiophene-benzothiadiazole for solar cells and transistors. Polym Chem. 2016;7:1549–58.
60. Huang H, Yang L, Facchetti A, Marks TJ. Organic and polymeric semiconductors enhanced by noncovalent conformational locks. Chem Rev. 2017;117:10291–318.